The International Archives of the Photogrammetry, Remote Sensing and Spatial Information Sciences, Volume L-4/W1-2026
Free and Open Source Software for Geospatial (FOSS4G) 2026 – Academic Track "Bridging Geospatial Technology and Humanity",
30 August–5 September 2026, Hiroshima, Japan

Rectangular vs Hexagonal Grid Tessellation for Spatial Analysis of Invasive Species: A Case Study of *Aromia bungii* in Saitama, Japan

Irhamillah Khamsim[1], Narumasa Tsutsumida [1,2], Hiroshi Tsunoda[3], Takeshi Osawa[4]

[1] Graduate School of Science and Engineering, Saitama University, Japan - irhamillahkhamsim@gmail.com
[2] Space Data Frontiers Research Center, Fujitsu Research, Fujitsu Limited, Japan - rsnaru.jp@gmail.com
[3] Faculty of Information Sciences and Collaborative Innovation, Nagano University, Japan - hiroshi-tsunoda@nagano.ac.jp
[4] Graduate School of Urban Environmental Sciences, Tokyo Metropolitan University, Japan - arosawa@gmail.com

Keywords: Hexagonal grid, rectangular grid, spatial autocorrelation, Moran's I, *Aromia bungii*, Saitama

Abstract

Aromia bungii has established persistent infestations across Saitama Prefecture, Japan, yet the influence of grid tessellation and spatial weight configuration on the detection of infestation clustering patterns remains poorly understood. This study evaluated whether rectangular (4,013 cells) and hexagonal (4,007 cells) tessellations, under four spatial weight configurations: Rook, Standard Queen, Distance-Weighted Queen, and Hexagonal KNN-6 yield consistent spatial autocorrelation results using 2,439 occurrence records spanning the years 2017–2024. Global Moran's I (0.4525–0.5380), Geary's C (0.5527–0.5970), and Getis-Ord G were all statistically significant ($p = 0.001$) across all configurations, confirming robust non-random clustering of *A. bungii* occurrence regardless of tessellation choice. Local autocorrelation analyses consistently identified two primary infestation hotspots: a cluster in the northern Kazo–Gyoda region and a localised cluster in the southeastern periphery of Saitama Prefecture across all configurations. Although hotspot locations were consistent across tessellation configurations, coldspot delineation was found to be unstable, with certain configurations producing inconsistent coldspot boundaries that may undermine the accurate identification of management priority zones. These findings provide a methodological basis for selecting appropriate tessellation structures in invasive species spatial analysis and offer spatially explicit evidence to support targeted surveillance and management planning for *A. bungii* in Saitama Prefecture.

1. Introduction

Biological invasions represent a major threat (Simberloff et al., 2013; Haubrock et al., 2026) to biodiversity, ecosystem stability, and agricultural systems worldwide.Invasive species can alter ecological processes, damage native host plants, and cause substantial economic impacts (Diagne et al., 2021), particularly when they spread rapidly across urban and peri-urban landscapes (Štajerová et al., 2017).Spatial analysis plays an important role in understanding invasive species distribution and identifying spatial clustering patterns associated with invasion processes (Dormann et al., 2007).In Japan, the invasive red-necked longhorn beetle, *Aromia bungii*, has become a growing concern due to its destructive impact on *Prunus* species, including ornamental cherry (Urano et al., 2022), peach, and plum trees.*A. bungii* was first detected in Aichi Prefecture,Japan in 2012 and has expanded across several prefectures through both natural dispersal and human-mediated spread, including the transport of infested wood materials. (Tamura and Shoda-Kagaya, 2022)

In Saitama Prefecture, Japan, established populations of *A. bungii* were first detected in Soka City in 2013, where several hundred ornamental cherry trees are planted along the canal corridor (Tamura and Shoda-Kagaya, 2022). Among affected host species, ornamental cherry trees are particularly important because of their ecological, cultural, and economic value as both a source of tourism (Urano et al., 2022) and landscape resource in Japan.Due to the importance of preserving the ornamental cherry tree, the Cellular Automata (CA) model developed by Osawa et al. (2022) to predict *A. bungii* expansion in Saitama Prefecture incorporated three landscape variables: ornamental cherry tree density, total river length, and total road length that form, a spatially connected host resource that may facilitate stepping-stone dispersal of *A. bungii* once a population is established.

Understanding the spatial relationship between *A. bungii* infestation and landscape features is critical for prioritizing management interventions. Identifying areas where host tree infestation is spatially concentrated allows authorities to prioritize countermeasures, including surveillance, early intervention, quarantine measures, and eradication efforts (Ministry of Agriculture, Forestry and Fisheries Japan, 2024). Aggregating point observations into spatially contiguous areal units is a useful approach for meaningfully quantifying clustering patterns. This aggregation requires a tessellation; the division of the study area into a set of non-overlapping spatial units, which can take either a rectangular or hexagonal grid form. Rectangular and hexagonal grids produce different neighbourhood connectivity structures, yielding different spatial autocorrelation values even for the same underlying data (Anselin, 1995). Spatial autocorrelation is sensitive to tessellation choice, representing one manifestation of the Modifiable Areal Unit Problem (MAUP). Rectangular and hexagonal tessellations produce different spatial weight matrices, where rectangular grids relying on contiguity-based weights (rook or queen) or distance-based weights, whereas hexagonal grids employ k-nearest neighbour (KNN) connectivity with six equidistant neighbours per cell. The implications of tessellation-induced differences in spatial autocorrelation for *A. bungii* occurrence patterns have not yet been examined and constitute the central methodological gap.

Spatial autocorrelation analysis is widely used to investigate clustering patterns in ecological and invasion biology studies

because it statistically measures the similarity between neighbouring observation. While the autocorrelation value can indicate the presence of a clustering pattern, it can vary depending on how the spatial unit is defined. Rectangular and hexagonal tessellations define different neighbourhoods, produce different spatial weights matrices (Anselin, 1988), and therefore yield different Moran's I values for identical underlying infestation data (Jelinski and Wu, 1996; Openshaw, 1984). The choice of tessellation geometry is particularly important when spatial autocorrelation results are intended to inform monitoring and eradication management strategies for invasive species.The choice of tessellation geometry also has direct ecological implications for representing organism movement and dispersal processes.When rectangular tessellations are used, neighbourhood relationships are inherently constrained to vertical and horizontal directions under Rook contiguity (Birch et al., 2007), or extended to diagonal directions under queen contiguity, though at unequal distances.This geometric constraint may restrict the representation of *A.bungii* dispersal, as this red-necked longhorn beetle is capable of moving in any direction when locating suitable host trees. In contrast, hexagonal tessellation provides six equidistant neighbours in all directions (Birch et al., 2007), more closely approximating the isotropic nature of actual movement and dispersal.By selecting a tessellation geometry that better reflects the biological movement process of the target species, researchers bring the spatial analysis closer to the ecological process of interest, thereby improving the ecological validity of the resulting clustering patterns and their practical relevance for invasion management. Conventional management approaches often prioritize confirmed hotspot regions, where infestation is already well-established and spatially concentrated. However, from an invasion management perspective, directing eradication efforts exclusively toward existing hotspot cores may be insufficient to prevent further spatial expansion. Transition zones located at the boundaries of established hotspot regions represent areas where infestation pressure is high but clustering has not yet fully developed, making them critical targets for early intervention before new clusters emerge.

The outcome of spatial statistical analysis can be influenced by the spatial unit used to aggregate geographic data, a phenomenon known as the Modifiable Areal Unit Problem (MAUP) (Openshaw, 1984).The MAUP manifests through two interrelated effects: (i) the scale effect, in which changing the size of spatial units alters statistical results, and (ii) the zoning effect, in which changing the shape or orientation of units of the same size also produces different outcomes (Jelinski and Wu, 1996).Both effects have been demonstrated to directly alter the computed values of spatial autocorrelation statistics, including Moran's I (Lee et al., 2019).In landscape ecology, Jelinski and Wu (1996) demonstrated that the choice of areal unit substantially changes both the magnitude and interpretation of clustering patterns through spatial autocorrelation analyses of vegetation data. Similarly, in disease mapping contexts, Lee et al. (2019) showed that the initial level of spatial autocorrelation at the finest scale plays a significant role in determining the nature and extent of MAUP effects on sample statistics, including means, variances, and Moran coefficients.

The sensitivity of spatial autocorrelation measures to tessellation geometry represents a manifeststation of the zoning effect, which is one of the components of MAUP.Zoning effects alter the results when different spatial partitioning schemes are applied to the same underlying dataset. In this study, different tessellation structures (rectangular and hexagonal) that represent zoning configurations produce different neighbourhood relationships and spatial weighting configurations. Therefore, any change in spatial autocorrelation measures can be interpreted as a zoning effect within the MAUP concept (Openshaw, 1984).

In general, rectangular grids are commonly used in spatial analysis because of their simplicity and direct compatibility with raster-based geographic data structures (Longley et al., 2011). Rectangular tessellations may introduce directional bias because diagonal neighbours are located farther than orthogonally adjacent neighbours, despite often being treated equally under queen contiguity schemes.In contrast, hexagonal tessellations provide more geometrically balanced neighbourhood relationships because all six neighbouring cells share equivalent edge lengths and equal centre-to-centre distances (Birch et al., 2007). These differences may influence the detection and interpretation of spatial clustering patterns.

Spatial autocorrelation measures include global Moran's I, Geary's C, and the Getis-Ord G statistics. The Getis-Ord G statistic does not account for spatial outliers and focuses exclusively on the concentration of hotspot and coldspot regions (Getis and Ord, 1992). Geary's C, in contrast, measures differences between neighbouring values and is more sensitive to local dissimilarities and boundary effects (Geary, 1954).

The objective of this study is to examine the influence of tessellation choice on spatial autocorrelation results.We evaluated the results using global and local spatial autocorrelation measures, as they provide comprehensive overview clustering tendencies. We investigated how the choice of tessellation geometries (rectangular vs hexagonal) influenced spatial autocorrelation analysis of *A.bungi* occurrence in Saitama Prefecture, Japan. We compared rectangular rook contiguity, rectangular queen contiguity, distance-weighted queen contiguity, and hexagonal tessellation using Global and Local Indicators of Spatial Association (LISA) to investigate how neighbourhood structure and grid geometry affect the measurement of spatial clustering.

2. Study Area and Data

Saitama Prefecture is located in the Kanto region of Honshu, Japan (Figure 1), covering a total land area of approximately 3,800 km bordered by Tokyo to the south. *A.bungii* data were collected by citizen science from 2017 to 2024, with a total of 2,439 incidence georeferenced points. All the incidence data have been verified by Center for Environmental Science in Saitama. The infestation was observed by citizen investigators during field surveys aimed at finding adult *A. bungii* or tree damage (i.e., the presence of frass excreted by *A. bungii* larvae on tree trunks) at that location.

3. Methods

3.1 Grid Construction

The rectangular grid was constructed at a resolution of 1 km $\times$ 1 km to cover the entire study area of Saitama Prefecture, yielding 4,013 grid cells projected in UTM Zone 54N (EPSG:32654). The hexagonal grid was generated by extending the rectangular grid construction algorithm to produce flat-top

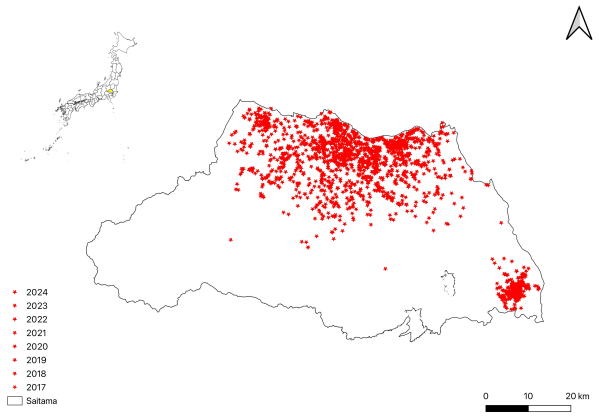

Figure 1. Study area: Saitama Prefecture, Japan, with red points representing *A.bungii* occurrence from 2017 until 2024.

regular hexagons covering the same spatial extent as the rectangular grid.Each hexagonal cell has a circumradius (equal to side length) of 620 m, a flat-to-flat diameter of 1,073.9 m, and a cell area of 0.999 km^2, yielding a total of 4,007 cells.This circumradius was selected to produce a cell area approximately equivalent to that of the 1 km × 1 km rectangular grid, ensuring comparable spatial resolution between two tessellations.

Hexagonal cells were constructed using Shapely and GeoPandas (Jordahl et al., 2020), with the method designed to be reproducible for any user-defined study area boundary. For both grid tessellations rectangular and hexagon, 2439 *A.bungii* occurence data from 2017 to 2024 were aggregated to grid cells, yielding 697 and 689 occurrence cells for rectangular (17.4%) and hexagonal (17.2%) cells, respectively.

3.2 Spatial Weight Configuration

Spatial autocorrelation analysis requires an explicit definition of neighbourhood relationships between spatial units. The definition of spatial weights matrix W, where each entry w_{ij} defines the degree of spatial interaction between cells i and j (Anselin, 1988) influences to the spatial autocorrelation analysis We therefore evaluated not only the effect of grid tessellation geometry (rectangular versus hexagonal), but also the effect of neighbourhood definition within the rectangular grid. Three rectangular weight configurations are compared: rook contiguity, standard queen contiguity, and distance-weighted queen contiguity and hexagonal KNN-6.

Four spatial weight configurations were evaluated in this study, as illustrated in Figure 2.

Rook contiguity (Figure 2a) assigns a weight of 1 to the four orthogonally adjacent neighbours (top, bottom, left, right) and excludes diagonal neighbours entirely. All four neighbours are at an equal distance of 1.0 km from the focal cell, making this the most geometrically consistent configuration for rectangular grids. Standard queen contiguity (Figure 2c) extends the neighbourhood to include all eight surrounding cells, assigning equal weights of 1 to both orthogonal neighbours (1.0 km) and diagonal neighbours (1.414 km).This treats geometrically unequal neighbours as equivalent, potentially introducing directional bias into spatial autocorrelation measures. Distance-weighted queen contiguity (Figure 2d) also

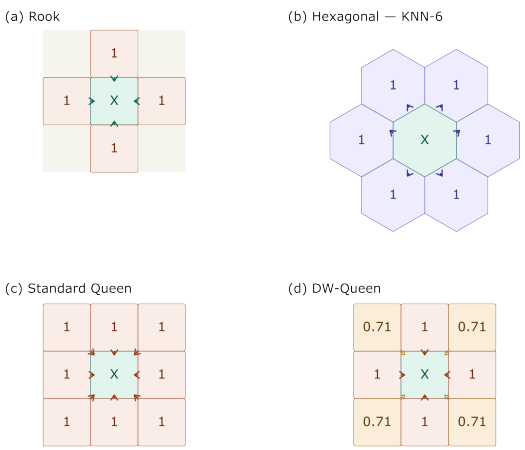

Figure 2. Spatial weight configurations: (a) Rook contiguity with 4 orthogonal neighbours; (b) Hexagonal KNN-6 with 6 equidistant neighbours; (c) Standard queen contiguity with 8 neighbours at equal weight; (d) Distance-weighted queen contiguity with diagonal neighbours weighted $1/\sqrt{2} \approx 0.707$.

considers all eight neighbours but corrects for the unequal distances by assigning diagonal neighbours a reduced weight of $1/\sqrt{2} \approx 0.707$, while orthogonal neighbours retain a weight of 1. This approach attempts to approximate geometric fairness within the rectangular grid framework.
Hexagonal KNN-6 (Figure 2b) assigns equal weights of 1 to all six neighbouring cells. Because all six neighbours share an equivalent edge length and are located at an equal centre-to-centre distance of approximately 1,073.9 m, this configuration inherently avoids directional bias without requiring any distance correction.

Configuration	Total grid cells	Neighbours	Orthogonal	Diagonal
Rook	4,013	4	1.000	—
Standard queen	4,013	8	1.000	1.000
DW-queen	4,013	8	1.000	0.707
Hexagonal KNN-6	4,007	6	1.000	n/a

Table 1. Summary of spatial weight configurations for rook, queen, distance-weighted (DW) queen, and hexagonal KNN-6. Note: "—" indicates that a parameter is not used in the configuration, whereas "n/a" denotes that the concept does not exist due to hexagonal geometry.

3.3 Spatial Autocorrelation Analysis

Spatial autocorrelation measures the degree to which a variable is correlated with itself across geographic space. Four spatial autocorrelation statistics were employed to evaluate comprehensively evaluate the spatial distribution of *A. bungii* occurrences across Saitama Prefecture. Global Moran's I (Moran, 1950) provides a single summary statistic of overall spatial clustering across the study area, calculated as:

$$I = \frac{n}{\sum_i \sum_j w_{ij}} \frac{\sum_i \sum_j w_{ij}(x_i - \bar{x})(x_j - \bar{x})}{\sum_i (x_i - \bar{x})^2}, \quad (1)$$

where n = number of spatial units

x_i, x_j = values of the variable $\boldsymbol{x}$ at locations i and j
$\bar{x}$ = mean value of the variable
w_{ij} = spatial weight between units i and j

Values of I range from -1 (perfect dispersion) to $+1$ (perfect clustering), with values near zero indicating spatial randomness. Statistical significance was assessed using a permutation-based approach with 999 permutations.

Local Moran's I (Anselin, 1988), a form of Local Indicators of Spatial Association (LISA), that identifies the decomposes the global statistic to identify the location and type of spatial clusters for each individual cell, calculated as:

$$I_i = \frac{x_i - \bar{x}}{s^2} \sum_j w_{ij}(x_j - \bar{x}), \tag{2}$$

where s^2 is the variance of $\boldsymbol{x}$. Each cell is classified into one of five categories based on its I_i value and statistical significance at $p < 0.05$ (based on 999 conditional permutations with a fixed random seed of 42 for reproducibility): High-High (HH, hotspot), Low-Low (LL, coldspot), High-Low (HL, spatial outlier), Low-High (LH, spatial outlier), and Not Significant (NS). All spatial autocorrelation analyses were conducted using the PySAL and ESDA libraries in Python (Rey and Anselin, 2007).

Geary's C (Geary, 1954) was used to emphasise local differences between neighbouring values rather than deviations from the global mean, calculated as:

$$C = \frac{(n-1)}{2\sum_i \sum_j w_{ij}} \frac{\sum_i \sum_j w_{ij}(x_i - x_j)^2}{\sum_i (x_i - \bar{x})^2}, \tag{3}$$

where a value of $C < 1$ indicates positive spatial autocorrelation (similar values cluster together), $C = 1$ indicates spatial randomness, and $C > 1$ indicates negative spatial autocorrelation (dissimilar values are adjacent).

Getis-Ord G statistic measures the concentration of high or low values within a specified distance (Getis and Ord, 1992), calculated as:

$$G = \frac{\sum_i \sum_j w_{ij} x_i x_j}{\sum_i \sum_j x_i x_j}, \quad j \neq i \tag{4}$$

The local G_i statistic (Ord and Getis, 1995) extends the global G to identify hot spots and cold spots at the individual cell level calculated as:

where S is the standard deviation of $\boldsymbol{x}$. A significantly positive G_i ($z > 1.96$) indicates a *hot spot*, spatial clustering of high values, while a significantly negative G_i ($z < -1.96$) indicates a *cold spot* spatial clustering of low values (Ord and Getis, 1995).

4. Results

We confirmed that the global spatial autocorrelation statistics were all positive and statistically significant (p = 0.001), indicating clustered spatial patterns across all four weight configurations in the study area (Tables 2).

Configuration	Moran's *I*	Geary's *C*	Getis-Ord G_i
Rook (4 neighbours)	0.5380	0.5527	0.0094
Standard Queen (diag=1)	0.4635	0.5970	0.0172
DW-Queen (diag=$1/\sqrt{2}$)	0.4525	0.5842	0.0172
Hexagonal KNN-6	0.4662	0.5919	0.0157

Table 2. Global spatial autocorrelation results for *A. bungii* occurrences under four spatial weight configurations.
All results statistically significant ($p = 0.001$). Moran's *I*: $I > 0$ = clustered. Geary's *C*: $C < 1$ = clustered.

Among the rectangular configurations, the Rook configuration yielded the highest Moran's *I* value (0.5380), followed by DW-Queen (0.4635) and Standard Queen (0.4525).This pattern may suggest that limiting neighbourhood definition to cardinal adjacency tends to produce a stronger clustering signal.The Hexagonal KNN-6 configuration returned a comparable value (0.4662), consistent with the rectangular results.

Figure 3 presents the cluster maps generated by local Moran's *I* across all four configurations. HH clusters, indicating localised concentrations of high *A. bungii* detection counts surrounded by similarly high neighbours, were consistently identified in two primary zones: the north-central and southeastern parts of Saitama Prefecture.HH cell counts ranged from 56 (Rook) to 70 (Hexagonal KNN-6). LL clusters were more spatially dispersed, appearing predominantly across the central and eastern portions of the prefecture, with counts ranging from 40 (Standard Queen) to 104 (Hexagonal KNN-6).High-Low (HL) and Low-High (LH) are spatial outliers categories, where HL cells indicate areas of high *A.bungii* occurrence surrounded by neighbours with low incidence reported, and vice versa for LH. Both outliers were found in minimal numbers across all configurations, suggesting limited spatial discontinuity within the detected clusters.

Figure 4 displays the Local Geary's *C* maps. Grids whose *A. bungii* counts were locally homogeneous with their neighbours were predominantly concentrated in the north-central region, consistent with the HH clusters identified by local Moran's *I*.Similar grids referring to those with homogeneous neighbour values ranged from 123 (DW-Queen) to 191 (Rook). Dissimilar grids having heterogeneous neighbour values where local counts contrast with the surrounding area, represent spatial boundaries or transitional zones between high and low detection areas, were found in relatively few cells across all configurations (48–60 cells), appearing mainly at the periphery of the identified clusters.Standard Queen and DW Queen shared the same values of dissimilar (53).

Figure 5 shows the Local Getis-Ord G_i hot and cold spots. Hot spots were consistently located in the north-central and southeastern regions across all configurations, with counts ranging from 70 (Rook) to 91 (Hexagonal KNN-6).Cold spots were more widely distributed across the central and eastern areas, ranging from 101 (DW-Queen) to 142 (Hexagonal KNN-6).The spatial extent of both hot and cold spots was broader under the Hexagonal KNN-6 configuration, eliminating isolated cells.

5. Discussion

The results demonstrate that tessellation choice influences both global and local spatial autocorrelation outcomes for *A. bungii* occurrences.Although all tessellation configurations showed

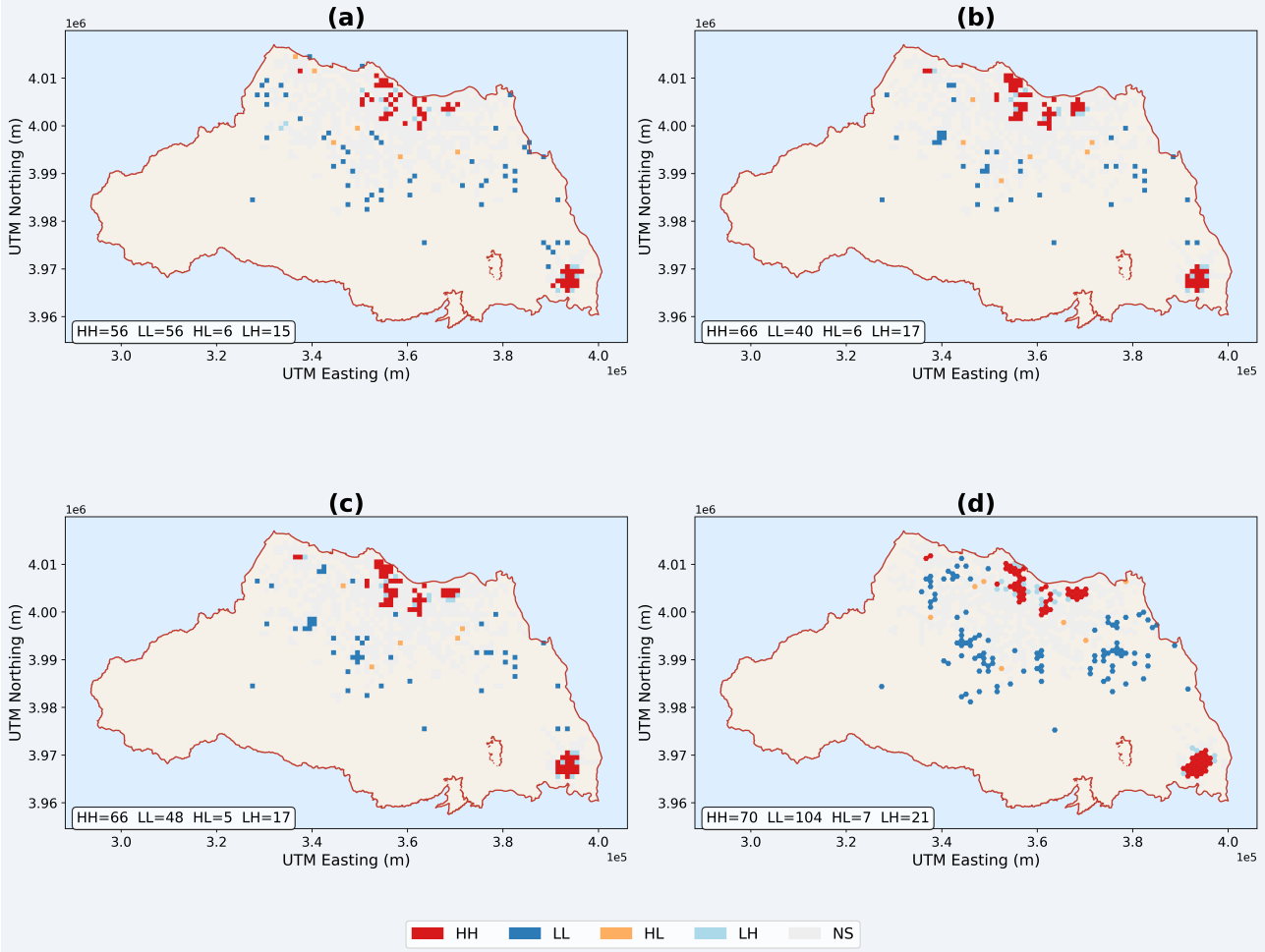

Figure 3. Local Moran's I cluster maps of *A.bungii* occurrences based on different spatial weight configurations: (a) Rook, (b) Standard Queen, (c) Distance-Weighted (DW) Queen, and (d) Hexagonal KNN-6.

statistically significant positive spatial autocorrelation according to global spatial autocorrelation measures, they differed in the magnitudes of the values foreach measure. The marginal variation in Moran's I across configurations suggests that the agglomeration is robust to the choice of spatial weight matrix, with clustering patterns remaining consistent despite differences in cluster counts.Major hotspot locations remained consistent across all tessellation configurations in the north-central and south-eastern regions of the study area, suggesting the robustness of clustering patterns to the neighbourhood structure choice.This confirms that spatial dependence exists, regardless of how neighbourhood relationships are defined.

At the local level, HH clusters identified through Local Moran's I, hotspot zones detected by Getis-Ord G_i, and similar cells identified through Local Geary's C were persistently located in the north-central and south-eastern regions across all configurations. This consistency confirms that the spatial structure of *A. bungii* infestation is stable and represents a genuine clustering pattern rather than a statistical artefact. Across all four tessellation configurations: Rook, Standard Queen, Distance-weighted Queen, and Hexagonal KNN-6, the primary hotspot locations remained unchanged, demonstrating that the detected spatial structure is robust to the choice of spatial weight matrix.The Hexagonal KNN-6 configuration classified the highest number of significant cells, attributable to its six-neighbour structure that encompasses greater spatial connectivity per cell compared to the Rook configuration (ecologically irrelevant spatial relationships), which considers only four neighbours. Despite these differences in neighbourhood arrangement, the core clustering pattern remained consistent, suggesting that the analytical results are not sensitive to tessellation type and can be considered reliable across spatial weight specifications.

LL clusters were spatially dispersed across the central and eastern portions of the study area, surrounding the primary HH clusters. This dispersed LL pattern may indicate transitional areas of low-level infestation situated between the identified hotspots and uninvaded areas. However, unlike HH clusters, the spatial distribution of LL clusters was not consistent across configurations, with the Hexagonal KNN-6 configuration detecting substantially more LL cells compared to other configurations, suggesting that LL classification is more sensitive to the choice of neighbourhood structure. From a pest management perspective, these low-density infestation zones deserve continued monitoring as they may represent areas of potential infestation risk. The dispersed distribution of infestation areas, combined with the predominance of similar cells in the Local Geary's C suggests that *A.bungii* does not establish new populations in distant areas but instead spreads gradually into neighbouring areas, which may be consistent with the short-range natural dispersal behaviour documented for *A.bungii* (EPPO, 2014).

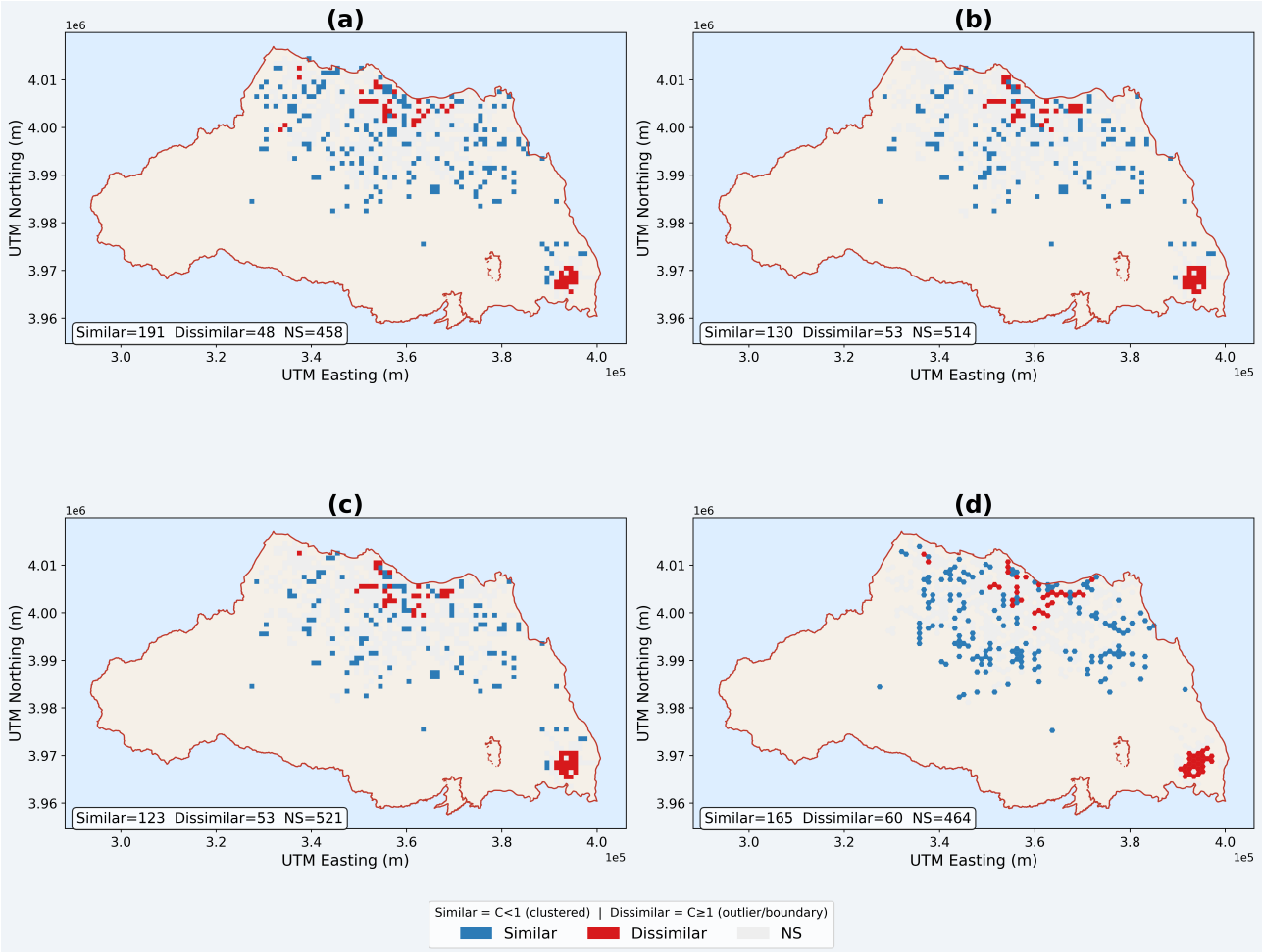

Figure 4. Local Geary's C cluster maps of *A.bungii* occurrences based on different spatial weight configurations: (a) Rook, (b) Standard Queen, (c) Distance-Weighted (DW) Queen, and (d) Hexagonal KNN-6.

Coldspot distributions varied considerably across configurations, ranging from 100 cells (DW-Queen) to 140 cells (Hexagonal KNN-6), due to differences in spatial weight configuration. This inconsistency renders it challenging to delineate priority protection areas as the spatial extent of coldspots is sensitive to the choice of neighbourhood structure. Within identified hot spot zones, management priorities may include the removal and destruction of heavily infested trees to reduce local population sources, combined with insecticide treatments targeting adults on surviving host trees to limit further egg-laying (oviposition) on healthy bark (EPPO, 2014).Concurrently, the surrounding cold spot and LL cluster zones may warrant enhanced surveillance to detect early-stage infestation before population levels escalate, as the short-range dispersal behaviour of *A. bungii* suggests that these peripheral zones represent areas at immediate risk of transitioning to higher infestation levels.

Hexagonal tessellation produced higher counts of similar cells associated with HH clusters compared to rectangular configurations due to six- neighbourhood structure equidistant by design, ensuring the spatial relationships are evaluated uniformly in all directions thereby reducing directional bias. In contrast, rectangular configurations evaluate neighbours at unequal distances, introducing directional bias that result in fragmented cluster boundaries and lower HH cell counts. Practitioners should therefore consider the tessellation configuration carefully when interpreting spatial cluster results for management planning, as different configurations may lead to different prioritisation of monitoring and eradication efforts, specifically at cold spot areas.

Several limitations should be acknowledged. Although comparable spatial resolutions were used, exact areal equivalence between rectangular and hexagonal tessellations could not be perfectly achieved due to their differing geometric structures. In addition, individual occurrence observations were aggregated into 1 km tessellation cells prior to analysis, meaning that the influence of the cell resolution and tessellation geometry on the detected spatial pattern could not be fully assessed in the present study.

6. Conclusions

This study examined the effects of tessellation geometry and spatial weight configuration on the detection of spatial autocorrelation in *Aromia bungii* occurrence data across Saitama Prefecture, Japan, using 2,439 positive detection records spanning 2017 to 2024. Two grid tessellations, rectangular (4,013 cells, 1.0 km^2 each) and hexagonal (4,007 cells, 0.9987 km^2 each), were used and evaluated under four spatial weight configurations: Rook, Standard Queen, Distance-Weighted Queen, and Hexagonal KNN-6.

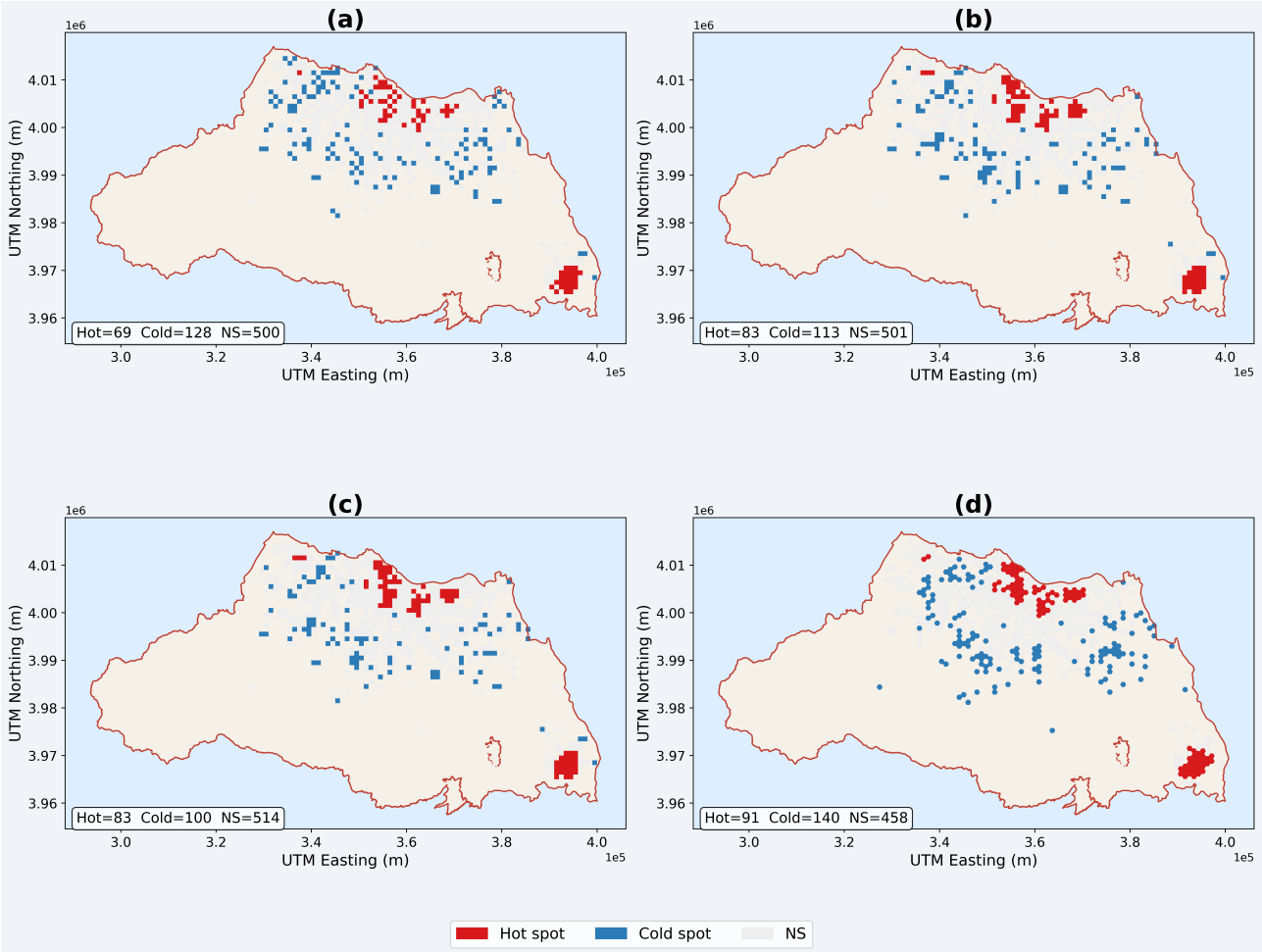

Figure 5. Getis-ord G_i cluster maps of *A.bungii* occurrences based on different spatial weight configurations: (a) Rook, (b) Standard Queen, (c) Distance-Weighted (DW) Queen, and (d) Hexagonal KNN-6.

Global spatial autocorrelation analysis confirmed significant and positive clustering of *A. bungii* occurrences across all configurations (Moran's $I = 0.4525$–0.5380, Geary's $C = 0.5527$–0.5970, Getis-Ord $G > 0$; all $p = 0.001$), demonstrating that the spatial agglomeration characteristic is robust to the choice of tessellation geometry and neighbourhood definition. Local spatial autocorrelation analyses consistently identified two primary hotspot zones at the northern (Kazo–Gyoda) and the southeastern (Soka) parts of Saitama Prefecture across all configurations, providing spatially explicit evidence of persistent infestation core that may serve as priority zones for targeted surveillance and countermeasure deployment.

More broadly, the results highlight that tessellation selection is not a neutral methodological decision in invasive species analysis. As tessellation selection directly determines neighbourhood structure, which in turn governs spatial connectivity, the choice of tessellation consequently influences the stability of coldspot delineation across the study area.Under different tessellation configurations, coldspot boundaries were found to be inconsistent, indicating that spatial clustering outcomes are sensitive to tessellation choice. This instability carries practical implications, as cold spot areas that are inconsistently identified risk transitioning into hotspots if left unmanaged.The study therefore provides practical guidance for selecting appropriate tessellation structures according to specific analytical objectives, such as eradication planning and local monitoring.

Acknowledgements

We appreciate the Center for Environmental Science in Saitama for providing the occurrence data of *Aromia bungii*. This study was funded by JSPS KAKENHI (25K09170).

References

Anselin, L., 1988. *Spatial Econometrics: Methods and Models*. Kluwer Academic, Dordrecht.

Anselin, L., 1995. Local indicators of spatial association—LISA. *Geographical Analysis*, 27(2), 93–115.

Birch, C. P. D., Oom, S. P., Beecham, J. A., 2007. Rectangular and hexagonal grids used for observation, experiment and simulation in ecology. *Ecological Modelling*, 206(3–4), 347–359.

Diagne, C., Leroy, B., Vaissière, A.-C., Gozlan, R. E., Roiz, D., Jarić, I., Salles, J.-M., Bradshaw, C. J. A., Courchamp, F., 2021. High and rising economic costs of biological invasions worldwide. *Nature*, 592(7855), 571–576.

Dormann, C. F., McPherson, J. M., Araújo, M. B., Bivand, R., Bolliger, J., Carl, G., Davies, R. G., Hirzel, A., Jetz, W., Kissling, W. D., Kühn, I., 2007. Methods to account for spatial

autocorrelation in the analysis of species distributional data: a review. *Ecography*, 30(5), 609–628.

EPPO, 2014. Pest risk analysis for *Aromia bungii*. Technical Report 15-21043, European and Mediterranean Plant Protection Organization, Paris.

Geary, R. C., 1954. The Contiguity Ratio and Statistical Mapping. *The Incorporated Statistician*, 5(3), 115–145.

Getis, A., Ord, J. K., 1992. The Analysis of Spatial Association by Use of Distance Statistics. *Geographical Analysis*, 24(3), 189–206.

Haubrock, P. J., Everts, T., Abreo, N. A. S., Bojko, J., Deklerck, V., Dickey, J. W. E., Franco, A. C. S., García-Berthou, E., Katsanevakis, S., Kirichenko, N. I., Mammola, S., Nuñez, M. A., Parker, B., Scalera, R., Soto, I., Strubbe, D., Tarkan, A. S., Vilizzi, L., Adriaens, T., Balzani, P., Błońska, D., Briski, E., Brys, R., Burgess, A. L., Byers, J. E., Cano-Barbacil, C., Castaldelli, G., Dick, J. T. A., Dominguez Almela, V., Dimarco, R. D., Florencio, M., Kouba, A., Kourantidou, M., Kurtul, I., Martín-Forés, I., Morissette, O., Olden, J. D., Soares, B. E., Truszkowski, J., Verreycken, H., Kenis, M., Sousa, R., Britton, J. R., 2026. The impacts of biological invasions. *Biological Reviews*, 101, 1255–1310.

Jelinski, D. E., Wu, J., 1996. The modifiable areal unit problem and implications for landscape ecology. *Landscape Ecology*, 11(3), 129–140.

Jordahl, K., Van den Bossche, J., Fleischmann, M., Wasserman, J., McBride, J., Gerard, J., Tratner, J., Perry, M., Badaracco, A. G., Farmer, C., 2020. GeoPandas: Python tools for geographic data. Version 0.8.0.

Lee, S.-I., Lee, M., Chun, Y., Griffith, D. A., 2019. Uncertainty in the effects of the modifiable areal unit problem under different levels of spatial autocorrelation: a simulation study. *International Journal of Geographical Information Science*, 33(6), 1135–1154.

Longley, P. A., Goodchild, M. F., Maguire, D. J., Rhind, D. W., 2011. *Geographic Information Systems and Science*. 3rd edn, John Wiley & Sons, Hoboken, NJ.

Ministry of Agriculture, Forestry and Fisheries Japan, 2024. Information on *Aromia bungii* (kubiaka tsuya kamikiri). Accessed: June 2026.

Moran, P. A. P., 1950. Notes on Continuous Stochastic Phenomena. *Biometrika*, 37(1–2), 17–23.

Openshaw, S., 1984. *The Modifiable Areal Unit Problem*. Concepts and Techniques in Modern Geography, 38, GeoBooks, Norwich.

Ord, J. K., Getis, A., 1995. Local Spatial Autocorrelation Statistics: Distributional Issues and an Application. *Geographical Analysis*, 27(4), 286–306.

Osawa, T., Tsunoda, H., Shimada, T., Miwa, M., 2022. Establishment of an expansion-predicting model for invasive alien cerambycid beetle *Aromia bungii* based on a virtual ecology approach. *Management of Biological Invasions*, 13(1), 24–44.

Rey, S. J., Anselin, L., 2007. PySAL: A Python Library of Spatial Analytical Methods. *Journal of Statistical Software*, 25(11), 1–18.

Simberloff, D., Martin, J.-L., Genovesi, P., Maris, V., Wardle, D. A., Aronson, J., Courchamp, F., Galil, B., García-Berthou, E., Pascal, M., Pyšek, P., Sousa, R., Tabacchi, E., Vilà, M., 2013. Impacts of biological invasions: what's what and the way forward. *Trends in Ecology & Evolution*, 28(1), 58–66.

Štajerová, K., Šmilauer, P., Brůna, J., Pyšek, P., 2017. Distribution of invasive plants in urban environment is strongly spatially structured. *Landscape Ecology*, 32(3), 681–692.

Tamura, K., Shoda-Kagaya, E., 2022. Genetic Differences among Established Populations of *Aromia bungii* (Faldermann, 1835) (Coleoptera: Cerambycidae) in Japan: Suggestion of Multiple Introductions. *Insects*, 13(2), 217.

Urano, T., Taki, H., Shoda-Kagaya, E., 2022. Comparison of the ecological traits and boring densities of *Aromia bungii* (Faldermann, 1835) (Coleoptera: Cerambycidae) in two host tree species. *Insects*, 13(2), 151.